BDS-3 precise orbit and clock solution at Wuhan University: status and improvement

Article *in* Journal of Geodesy · February 2023

DOI: 10.1007/s00190-023-01705-5

Journal of Geodesy (2023) 97:15
https://doi.org/10.1007/s00190-023-01705-5

ORIGINAL ARTICLE

BDS-3 precise orbit and clock solution at Wuhan University: status and improvement

Jing Guo[1] · Chen Wang[1,3] · Guo Chen[1] · Xiaolong Xu[1] · Qile Zhao[1,2]

Received: 6 August 2020 / Accepted: 24 January 2023

Abstract
With the rapid deployment of the third-generation satellites of the BeiDou Navigation Satellite System (BDS-3), Wuhan University (WHU) has incorporated BDS-3 satellites to its routine Multi-GNSS analysis since Day of Year 1, 2019. This article summarizes the processing strategy and presents the validation results of the WHU BDS-3 orbit and clock solutions submitted to the International GNSS Service Multi-GNSS Experiment in 2019. Although more than 200 stations with B1I and B3I signals tracking capability can be used for BDS-3 precise orbit determination, the number of tracking stations for different satellites diverges greatly; in general, more stations track those launched early and less those deployed late. The validations with orbit boundary misclosures, orbit differences with respect to BDS-3 products of GeoForschungsZentrum (GFZ) and Satellite Laser Ranging (SLR) residuals show that the orbits are affected by the number of tracking stations and the deficiency of dynamic models. To overcome the latter, an a priori solar radiation pressure (SRP) model has been proposed considering the Earth albedo and antenna thrust. The SLR validation shows that the new SRP model significantly improves the orbit from 5 to 7 cm to about 3 to 4 cm by reducing the Sun-elongation-angle-dependent errors of the BDS-3 orbits. Besides, the clock products have been compared with those of GFZ, and the root-mean-square (RMS) of clock linear fit is also analyzed. Noticeable different quality has been shown for Rubidium Atomic Frequency Standard and Passive Hydrogen Maser (PHM) clocks. The Sun-elevation-angle-dependent patterns are identified in PHM clocks, and the RMS of clock linear fit of PHM clocks can be reduced with improved dynamic modeling, particularly in eclipse seasons.

Keywords BDS-3 · Precise orbit determination · Clock · Solar radiation pressure · Metadata

1 Introduction

As one of the analysis centers (ACs) of the International GNSS Service (IGS, Johnston et al. 2017), Wuhan University (WHU) has been contributing to the IGS for providing ultra-rapid as well as rapid orbit and clock solutions of the established GPS and GLONASS since 2012. In the same year, the IGS initiated the Multi-GNSS Experiment (MGEX) to support the analysis of the emerging GNSS systems and prepare the IGS for Multi-GNSS (Montenbruck et al. 2017), which includes GPS, GLONASS, the European Galileo system, the Chinese BeiDou Navigation Satellite System (BDS), the Japanese Quasi-Zenith Satellite System (QZSS) and the Indian Regional Navigation Satellite System (IRNSS/NaVIC).

Initially, the focus of WHU's MGEX-related activity was on the analysis of the BDS performance. After the success of the initial BeiDou demonstration navigation system (BDS-1), China has started to construct the regional BDS (BDS-2) since 2009. With the massive deployment of satellites in the next three years, positioning, navigation, and timing (PNT) service could be declared for BDS-2 around the Asia–Pacific region at December 27, 2012. With the support of the BeiDou Experimental Tracking Network (BETN) established by WHU, the orbit and clock solutions for BDS-2 satellites have been determined and submitted to IGS MGEX since 2012. 2013 was the first year when quad-constellation, i.e., GPS, GLONASS, Galileo, and BDS, was included in WHU's

✉ Chen Wang
chen.wang@whu.edu.cn

1 GNSS Research Center, Wuhan University, No. 129 Luoyu Road, Wuhan 430079, China

2 Collaborative Innovation Center of Geospatial Technology, No. 129 Luoyu Road, Wuhan 430079, China

3 School of Geological Engineering and Geomatics, Chang'an University, 126 Yanta Road, Xi'an 710064, China

Published online: 09 February 2023

MGEX (WUM) solution by using the BETN and increasing MGEX network. Later, the QZSS Michibiki satellite has been incorporated into the WUM solution since 2015. The dynamic models and analysis strategies employed for the WUM solution have been first presented in Guo et al. (2016) and were updated later (Guo et al. 2018). The updates in the fields of orbit modeling include usages of the a priori solar radiation pressure (SRP) model for BDS-2 GEO (Wang et al. 2019a), Galileo (Montenbruck et al. 2015a) and QZSS Michibiki (Zhao et al. 2018) satellites to augment the deficiencies of the 5-parameter Extended CODE Orbit Model (called ECOM1 in this study, Beutler et al. 1994), activating the antenna thrust for Galileo, GPS and GLONASS with transmit power value from Steigenberger et al. (2018), and modeling the Earth albedo for GPS, GLONASS and Galileo satellites with the dimensions and optical properties released by European GNSS Service Center (GSC 2017). Besides, the eclipse yaw laws were considered for BDS, QZSS and Galileo satellites, and the transmit antenna calibrations from the estimation or metadata were applied instead of the MGEX recommended values. The analysis summary file with the changes of WUM solution in detail up to June 2020 can be accessed at https://igs.org/mgex/data-products.

Since 2015, five experimental satellites of the global BDS system (BDS-3s) were launched to serve as technology validation for the new features of BDS-3, including signals, inter-satellite link (ISL) technology and onboard frequency standards. Two years later, the first operational satellite of the global BDS system (BDS-3) was launched on December 5, 2017. The following launches in 2018 resulted in a rapid increase of the number of BDS-3 satellites allowing China to announce the achievement of operational capability on December 27, 2018, when there were 18 Medium Earth Orbit (MEO) and 1 Geostationary (GEO) satellites in orbit. Different with BDS-2 that were manufactured by or not China Academy of Space Technology (CAST), BDS-3s/BDS-3 satellites are manufactured by CAST as well as Shanghai Engineering Center for Microsatellites (SECM) of the China Academy of Science (CAS). With the development of the BDS-3 constellation, the tracking networks from the International GNSS Monitoring and Assessment System (iGMAS; Jiao and Liu 2014) and IGS have been upgraded gradually to track BDS-3 signals. This laid the fundament for the analysis of BDS-3. Hence, since Day of Year (DOY) 1, 2019, BDS-3 satellites have been incorporated in WUM routine analysis. Although some efforts have been put to investigate the characteristics of BDS-3, e.g., the eclipse yaw laws (Zhao et al. 2017; Wang et al. 2018), we consider the state as preliminary and the starting point for BDS-3 analysis. The analysis of the extended time series of WUM BDS-3 products allows us to identify weaknesses and to seek for better strategies and models for BDS-3 data processing.

Previously, some new characteristics and modeling deficiencies of BDS-3 have been investigated and analyzed. The noticeable improvement is that the satellite-specific code biases have been eliminated for BDS-3 satellites (Zhang et al. 2017; Zhou et al. 2018). And the performance of onboard Rubidium Atomic Frequency Standard (RAFS) clocks is improved further, while the Passive Hydrogen Maser (PHM) clocks show even better performance (Zhang et al. 2019). The ISL data have been analyzed and used for precise orbit determination (POD) of BDS-3 in combination with ground L-band data or without (Yang et al. 2017; Tang et al. 2018; Xie et al. 2019; Wang et al. 2019b). For the modeling deficiencies, the Sun-elongation-angle-dependent systematic errors in Satellite Laser Ranging (SLR) residuals of CAST MEO satellites were identified by Dilssner et al. (2018), and later on, Yan et al. (2019) found this kind of errors in the orbits of SECM MEO satellites too. Similar as Galileo and QZSS, this pattern is supposed to be due to the cuboid shape of satellites with relatively high area-to-mass ratio (Sośnica et al 2020) and can be reduced significantly by using the empirical ECOM-2 (Arnold et al. 2015) or an a priori semi-analytical model (Yan et al. 2019; Wang et al. 2019) as well as a box-wing model based on the released or calibrated metadata (Li et al. 2020a; Duan et al. 2021).

The main goal of this work is to present the analysis strategy we use for BDS-3 and evaluate the quality of orbit and clock solutions to identify the weaknesses of the strategy for seeking for improvements. We start with the description of the status of the BDS-3 constellation as well as the tracking network, and metadata consisting of sizes and optical properties of the main satellite surfaces, eclipse attitude laws and transmit antenna calibrations from China Satellite Navigation Office (CSNO) in Sect. 2. Section 3.1 describes the analysis strategy used for the generation of WUM BDS-3 orbit and clock solutions as well as the reprocessed orbits in this study based on the improved models. In Sect. 3.2, the operational WUM BDS-3 products are analyzed by using orbit boundary misclosures, SLR validation and comparison with the BDS-3 solutions from Deutsches GeoForschungsZentrum (GFZ) MGEX AC. The model improvements and reprocessed solutions are presented and validated in Sect. 4. Finally, the results are summarized and discussed in Sect. 5.

2 Status of BDS-3 constellation and data

2.1 BDS-3 constellation

With the last GEO satellite launched on June 23, 2020, the BDS-3 constellation, consisting of 24 MEO, 3 GEO and 3 Inclined Geosynchronous Orbit (IGSO) satellites, has

Table 1 The status of BDS-3 constellation on December 20, 2022

Satellite type	Manufacture	# of satellites	Primary Clock type	Secondary Clock type	Signals
GEO	CAST	3	PHM	RAFS	RNSS: B1I/B3I PPP: B2b SBAS: B1C/B2a
IGSO	CAST	3	PHM	RAFS	RNSS: B1I/B3I/B1C/B2a SAR: B2b
MEO	CAST	14	RAFS (before 2019), PHM	RAFS	
	SECM	10	PHM	RAFS	

CAST China Academy of Space Technology, *SECM* Shanghai Engineering Center of Microsatellites, *RAFS* Rubidium Atomic Frequency Standard, *PHM* passive hydrogen maser, *RNSS* radio-based navigation satellite system, *PPP* precise point positioning, *SBAS* satellite-based augmentation system, *SAR* search and rescue

been completed half a year ahead of the scheduled deadline (CSNO 2018). Among the satellites, 3 GEO, 3 IGSO and 14 MEO manufactured by CAST have been successfully deployed, whereas 10 MEO satellites from SECM also provide PNT services. For SECM MEO satellites, two Chinese PHM clocks are used as the primary frequency standard, while two improved Chinese RAFS clocks are used as backup. For CAST MEO satellites launched before 2019, the four RAFS clocks are used as the primary and backup, whereas the two PHM clocks are used as the primary frequency standard for CAST GEO, IGSO, and the rest MEO satellites. Table 1 lists status of the BDS-3 constellation on July 13, 2020. The reader can refer to the website of the Test and Assessment Research Center (TARC) of CSNO for the latest status of BDS system (http://www.csno-tarc.cn/system/constellation).

According to Yang et al. (2018), BDS-3 satellites broadcast eight signals in B1, B2 and B3 bands. The B1 band signals centered at 1575.42 MHz include an open service (OS) B1C signal and an authorized service (AS) B1A signal, as well as a BDS-2 backward compatible B1I signal at 1561.098 MHz. The B2 band transmits two OS signals, i.e., B2a at 1176.45 MHz and B2b at 1207.14 MHz. The B2b signal plus B2a signal together forms a B2 signal on 1191.795 MHz. The B3 band contains an AS B3A signal centered at 1268.52 MHz, as well as the BDS-2 compatible B3I signal. All of the BDS-3 satellites broadcast these signals to provide Radio Navigation Satellite Service (RNSS), whereas three GEO satellites provide Satellite-Based Augmentation System service on OS B1C/B2a and AS B1A signals. Besides, the state-space-representation (SSR) corrections of orbit, clock and code biases are broadcasted to users in China and the surrounding area through the B2b signal of GEO satellites to support real-time precise point positioning (PPP). The global short message communication is provided via the B2b signal of the 14 MEO satellites with the support of ISL (Yang et al. 2019).

2.2 Satellite metadata

The metadata related to the BDS-2 and BDS-3 spacecrafts was disclosed by CSNO on December 09, 2019, and December 25, 2019 (CSNO 2019), respectively. The published BDS-3 metadata comprises mass, sizes and optical properties of the main satellite surfaces, eclipse attitude laws, laser retro-reflector array (LRA) and navigation antenna offset vectors with respect to the center of mass (CoM) in the satellite fixed reference frame. The availability of disclosed spacecraft metadata will lead to the improvement of orbit and clock determination of BDS-3, particularly for the orbit modeling. However, the specular and the diffuse reflection coefficients are not released which limits the modeling of SRP as well as Earth albedo based on an analytical model. With assumed specular and diffuse reflection coefficients for the main surfaces, Li et al. (2020a) assess the possibility of the disclosed metadata for defining a box-wing model suited for analytical SRP in combination with ECOM1, and the optical properties have been calibrated further (Duan et al. 2021). Moreover, the transmit power is necessary for modeling antenna thrust; although the values are not disclosed by CSNO, they are measured and estimated as 310 W and 280 W for CAST and SECM MEO satellites by Steigenberger and Thoelert (2020). As to the yaw attitude, the released eclipse attitude laws predict the yaw behaviors of SECM satellites during eclipse seasons quite well, whereas the models proposed by Dilssner (2017) and Wang et al. (2018) work better for CAST satellites.

2.3 Tracking stations

The ground L-band tracking data from IGS and iGMAS network can be obtained and used for BDS-3 analysis. Figure 1 shows the global distribution of ground stations with BDS-3 tracking capability from these two networks at DOY 364, 2019. For the totally 25 stations of the iGMAS network, there are mainly five kinds of receivers, i.e., GMR-4011,

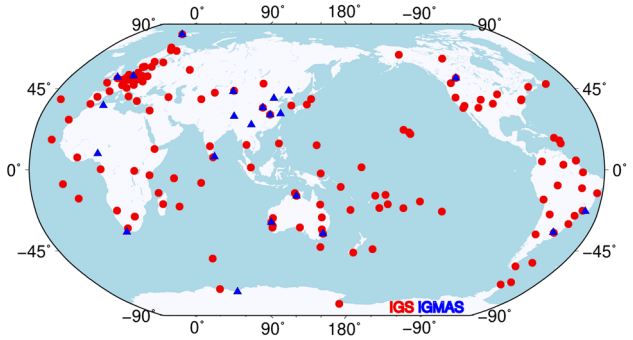

Fig. 1 The distribution of ground stations with BDS-3 tracking capability from iGMAS (blue triangle) and IGS (red dots) networks at DOY 364, 2019

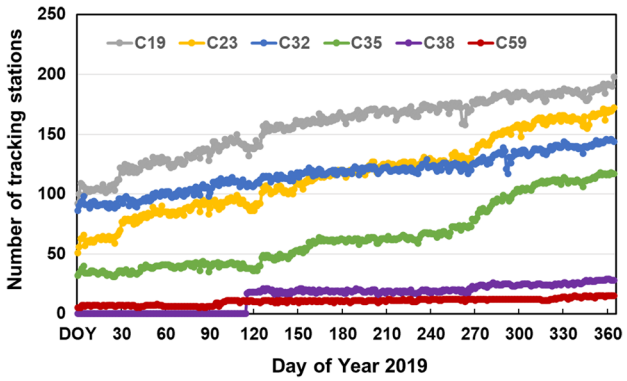

Fig. 3 The daily number of IGS and iGMAS stations tracking the representative BDS-3 satellites C19, C23, C32, C35, C38 and C59 in 2019

GMR-4016 and GNSS-GGR from the 20th and 54th Institute of China Electronics Technology Corporation as well as UB4B0I and UB4B0-13478 from Unicore Co. Ltd, respectively. One additional receiver BD070 is from National University of Defense Technology (NUDT). All receivers support tracking of the B1I, B3I, B1C and B2a OS signals from all deployed BDS-3 satellites. Furthermore, the B2b signal can be tracked by GNSS-GGR and BD070 receivers. With the release of the interface control documents (ICDs) for BDS-3 signals, the GNSS receivers of the IGS network are gradually upgraded tracking BDS-3 signals. In general, 9 types of receivers from Septentrio, Trimble, Javad and Leica support tracking the backward-compatible B1I and B3I signals. Moreover, Javad TRE_3 and Trimble Alloy can track all BDS-3 OS signals. Figure 2 shows the daily number of IGS and iGMAS stations tracking BDS-3 satellites in 2019. At the beginning of 2019, there are 93 and 19 stations from IGS and iGMAS network with BDS-3 B1I and B3I signals tracking capability, and it increases to 171 and 25 by the end of 2019 due to deployment of Trimble Alloy and updates of Trimble NetR9, Septentrio POLARX5/POLARX5TR as well as receivers of iGMAS network.

However, not all deployed BDS-3 satellites can be tracked by each receiver, possibly due to the limitation of tracking channels or firmware. Figure 3 shows the daily number of IGS and iGMAS stations tracking representative satellites C19, C23, C32, C35, C38 and C59, in 2019. The number of stations with C19 tracking capability represents those for satellites C19–C22, whereas those tracking C23 indicates the number of stations for satellites C23–C31 and similar for the remaining. Although the pseudo-random-noise (PRN) number is not a unique satellite identifier as satellite vehicle number (SVN), the BDS PRN assignment stayed unchanged in 2019. Hence, the PRN is used as the satellite identifier in this study. In general, the early launched satellites can be tracked by more receivers. At the beginning of 2019, except for Javad TRE-3 Delta and iGMAS receivers with ability to track all deployed BDS-3 satellites, Trimble receivers can only track the satellites C19–C30, and Septentrio receivers with latest firmware can only track satellites C19–C22 and C32–C34. Hence, the number of stations with C19 tracking capability is the highest followed by C32. With the upgrade of Trimble NetR9 as well as deployment of Trimble Alloy, the number of stations tracking C23 increases gradually and even exceeds that of C32. Thanks to the upgrade of Septentrio

Fig. 2 The daily number of IGS and iGMAS stations with BDS-3 tracking capacity in 2019

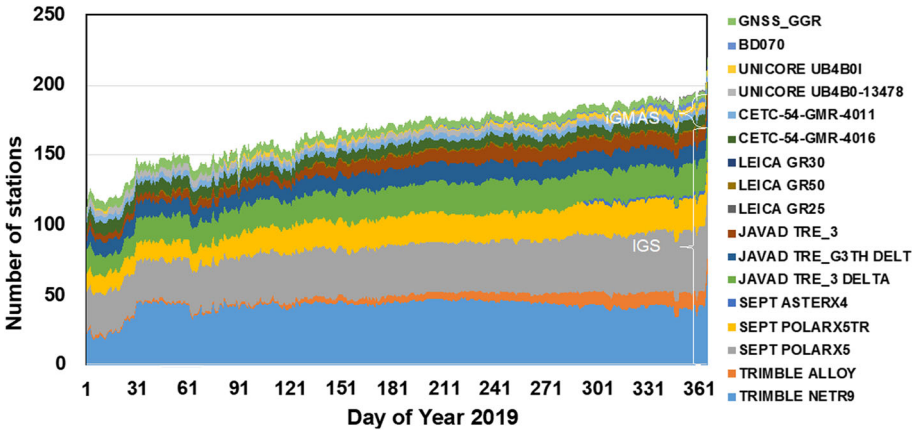

firmware, C35 is tracked by more stations, and the number exceeds 100 by the end of 2019. IGSO and MEO satellites with PRN beyond 40 are tracked only by iGMAS stations in 2019.

3 WUM BDS-3 orbit and clock products

3.1 Strategy

The analysis strategy used for generating WUM products has been first described by Guo et al. (2016), and the relevant changes until the end of 2018 were summarized in Guo et al. (2018). Following the launch of three QZSS-2 satellites in June 2017, QZSS completed a four-satellite constellation and announced an official start to provide service in November 2018. Meanwhile, the global PNT service provided by BDS-3 satellites was announced at the end of 2018. Hence, the BDS-3 and QZSS-2 satellites have been incorporated into the WUM routine analysis since DOY 1, 2019, when the frequencies used for BDS data processing were switched from B1I/B2I to B1I/B3I. This choice is driven initially by two facts, (1) most of the receivers from the IGS network can only track the two backward compatible signals for BDS-3, and (2) the common signals facilitate the integrated processing of BDS-2 and BDS-3 for both orbit determination as well as positioning. Considering that no more than 30 stations are available with ability of tracking the signals from the three IGSO satellites as well as the MEO satellites with PRN beyond C38 in 2019, they have not been included for analysis until DOY 279, 2020. Besides, the GEO satellites, i.e., C59, C60 and C61, are not analyzed due to poor tracking geometry as well as deficiencies in orbit modeling. The calibrated phase center corrections (PCCs) of BDS-2 from Guo (2014) as well as the satellite-specific PCO from CSNO (2019) for BDS-3 have been used until GPS week 2072, when the block-specific PCOs in the IGS official antenna file are used for all constellations. For receiver antenna corrections, as ground antenna calibrations covering all GNSS and all frequencies are not available to the IGS until recently, the PCCs for the new constellations are adopted from the GPS L1 and L2 frequencies. The orientation of BDS-3 satellites in space follows the conventions in Montenbruck et al. (2015b) considering eclipse yaw laws presented in Wang et al. (2018) and Lin et al. (2018) for BDS-3 CAST and SECM satellites, respectively. For the non-conservative perturbations, the ECOM1 SRP model is used without considering any a priori model, whereas the Earth albedo and transmit antenna thrust are omitted. Moreover, the ambiguities are fixed for BDS-2 and BDS-3 with considering as a single constellation with excluding the GEO satellites (Li et al. 2019). The whole data processing for POD of WUM products is processed with a modified version of Position And Navigation Data Analyst software (PANDA; Liu and Ge 2003). Table 2 summarizes the measurement and orbit dynamic models for WUM BDS-3 data analysis before June 2020.

Table 2 Summary of the models and strategies applied for WUM BDS-3 analysis before June 2020

Observable	Undifferenced ionosphere-free code and phase combination of B1I and B3I
POD arc length	24 h
Sampling rate	300 s
Elevation angle cutoff	10°
Weighting	$e > 30°$: 1; $e \leq 30°$: 2*sin(e)
Satellite antenna PCO/PCV	igs14_wwww.atx since week 2072; WHU estimation for BDS-2 (Guo et al. 2016), and CSNO release for BDS-3 used before week 2072 (CSNO 2019)
Receiver antenna PCO/PCV	GPS L1 and L2 corrections
Ambiguity resolution	Fixed to integer (Ge et al. 2005)
Satellite yaw attitude	GEO: Orbit normal mode IGSO: nominal yaw-steering mode CAST MEO: Wang et al. (2018) SECM MEO: Lin et al. (2018)
Geopotential	EGM2008 with degree and order 12 (Pavlis et al. 2012)
Tidal variations in geopotential	Solid earth tides: IERS conventions 2010 (Petit and Luzum 2010)
	Ocean tides: not applied
	Solid earth pole tide: IERS conventions 2010 (Petit and Luzum 2010)
	Ocean pole tide: IERS conventions 2010 (Pavlis et al. 2012)
Third-body	Sun, Moon, Mercury, Venus, Mars, Jupiter, Saturn, Uranus, Neptune, Pluto JPL Planetary Ephemeris DE405 (Standish 1998)
SRP model	5-parameter ECOM without a priori SRP model
Earth albedo	Not applied
Antenna thrust	Not applied
Relativistic effects	Schwarzschild and lense-thirring effects

BDS-2 and BDS-3 are treated as one constellation in WUM; hence, only one inter-system bias is estimated from their measurements with respect to GPS. Recently, Mi et al. (2021) clearly show the existence of system-specific receiver code biases between BDS-2 and BDS-3 overlapping signals, i.e., B3I. The estimates of parameters will be

contaminated, once the bias is not properly handled. For the reprocessed solution in this study, a similar strategy is used for WUM, but two ISB parameters are estimated to consider the system-specific receiver code biases between BDS-2 and BDS-3. The intra-constellation double-difference ambiguities within BDS-2 or BDS-3 are formed for ambiguity resolution, instead of forming inter-system ambiguities (Peng et al. 2022). Besides, for satellite C35–C37, the measurements are low at the first half of 2019; hence, ambiguity parameters are not well determined. They may easily be fixed to the wrong values resulting in a fixed solution with lower quality. Hence, the data of C35–C37 after DOY 180, 2019, are analyzed.

3.2 Orbit quality

The WUM BDS-3 orbit and clock products for the full year 2019 are selected for analysis. As aforementioned, only MEO satellites were analyzed in this period, the validation of orbits and clocks of IGSO and GEO satellites is not performed in this study. During this period, GFZ also has released their BDS-3 solutions since DOY 322, 2019, at their ftp server (ftp://ftp.gfz-potsdam.de/GNSS/products/mgex), and the European Space Operations Centre of the European Space Agency (ESA) has also been providing BDS-3 orbit and clock solutions since DOY 1, 2019 (http://navigation-office.esa.int/products/gnss-products/). The orbit differences between WUM and ESA solutions have been assessed by Li et al. (2020b). Hence, to assess the quality of WUM BDS-3 orbits, the metrics including orbit boundary disclosures (OBD), SLR validation, and comparison with GFZ solutions are used.

3.2.1 Orbit boundary disclosures

As an internal validation of orbit quality, OBD has been proposed by Griffiths and Ray (2009) using 3D position differences at the overlapping epoch to assess the orbit accuracy. Intrinsically, this approach is similar as overlapping orbit differences to validate the consistency of consecutive orbits from the same AC, but it does not give overly optimistic results since only one orbit position at a specific epoch is used for comparison. In this study, the position differences at the midnight epoch of two adjacent 24-h POD arcs were computed as OBD. Figure 4 presents the mean RMS of daily OBDs in along-track, cross-cross-track, radial directions and 3D for each BDS-3 satellite. As expected, the largest errors of up to about 57 cm (C35) are in along-track, whereas the radial orbit component shows the best consistency with maximum of about 14 cm (C35) and minimum of about 3.7 cm (C19). Besides, the noticeable correlation between OBD and the available tracking data can be identified. For satellites C19–C22 tracked by most stations, the best consistency is achieved, followed by C32–C34. The orbits of C35–C37

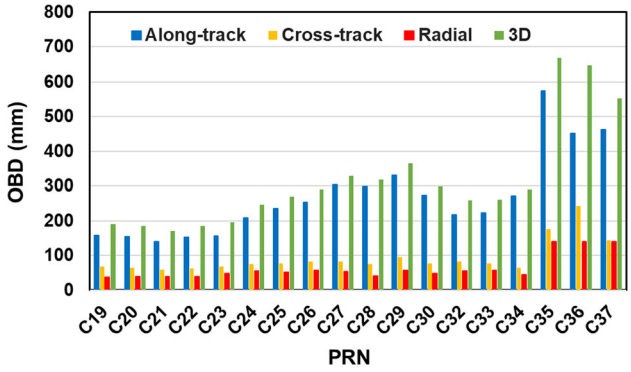

Fig. 4 The averaged RMS of orbit boundary disclosures in along-track, cross-track, radial directions and 3D for BDS-3 satellites

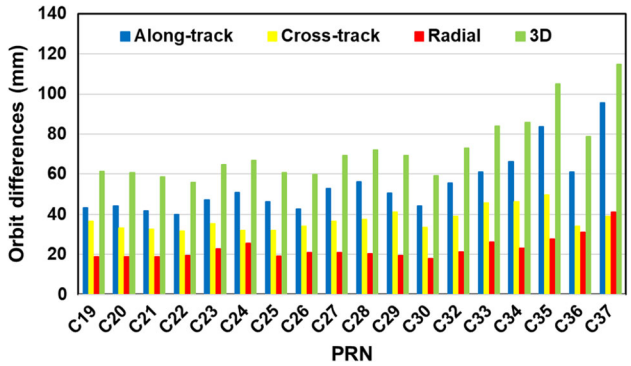

Fig. 5 The mean RMS of daily orbit differences between WUM and GFZ BDS-3 orbit solutions in along-track, cross-track, radial directions and 3D directions

show the worst performance due to fewest data available for analysis.

3.2.2 Differences to GFZ solutions

With the BDS-3 orbits from GFZ during DOY 323 to 365, 2019, as the reference, the orbit comparison is performed. Figure 5 shows the mean RMS of daily orbit differences in along-track, cross-track, radial directions and 3D directions for BDS-3 satellites. Generally, the achieved consistency between GFZ and WUM solution is better than 10 cm, 5 cm and 4 cm in along-track, cross-track and radial directions for all satellites. Like the OBDs, the satellites with fewer tracking data show lower consistency, in particular for satellites C35, C36 and C37. The average RMS for the three satellites is about 8.0 cm, 4.1 cm and 3.3 cm in along-track, cross-track and radial directions. It decreases by about 2.0 cm and 1.0 cm in along-track and radial components for satellites C32, C33 and C34, compared to C35–C37. For the group consisting of C19, C20, C21 and C22, the best consistency is achieved due to most tracking data available. The averaged RMSs are

Table 3 Statistics of the SLR residuals for WUM BDS-3 orbit solutions (unit: cm)

Manufacture	CAST		SECM	
PRN	C20	C21	C29	C30
Mean	4.04	4.04	− 4.52	− 4.92
STDev	3.83	3.87	4.55	4.39
RMS	5.57	5.59	6.49	6.59

4.2 cm, 3.4 cm and 1.9 cm in the three directions. For other satellites, slight degeneration is observed.

It is worth to mention that the consistency between ESA and WUM solutions has been assessed by Li et al. (2020b), and it is worse than that between GFZ and WUM, as ESA uses the in-house estimated PCO and PCV for BDS-3 instead of the IGS-recommended value used by GFZ and WUM (Springer et al., 2020). The lower consistency for SECM satellites than for CAST is mainly caused by the fewer measurements available.

3.2.3 SLR validation

SLR is used for independent validation of GNSS satellite orbits mainly in the radial component. All launched BDS-3 satellites are equipped with LRAs; however, only four of them, i.e., C20, C21, C29 and C30, are tracked by ILRS (Pearlman et al. 2019). And two out of them, i.e., C20 and C21, are manufactured by CAST, whereas the other two, i.e., C29 and C30, are from SECM. The offsets of the LRA with respect to CoM in the satellite reference frame released by CSNO (2019) for CAST and SECM missions are used. Table 3 summarizes the validation results. Residuals exceeding 0.5 m are treated as outliers and are removed, and the four-sigma threshold is used to further remove bad measurements. Finally, there are 2762, 3411, 2526 and 2398 out of 2782, 3430, 2559 and 2438 normal points available for C20, C21, C29 and C30, respectively.

It is clearly observed that CAST and SECM satellites show different performance, whereas almost the same accuracy is achieved for satellites from same manufacturers. For CAST satellites, the Standard Deviation (STDev) of SLR residuals is about 3.8 cm with positive bias up to 4.0 cm, making that the precision of orbits reaches about 5.6 cm. However, a negative bias beyond − 4.5 cm is identified for the SLR residues of SECM orbits, and slightly larger STDev (about 4.5 cm) than that of CAST is also observed. The accuracy of C29 and C30 orbits is about 6.5 cm, which is about 1.0 cm worse than that of the two CAST satellites, due to few tracking data available as shown in Fig. 3, particularly in the beginning of 2019.

Figure 6 shows the SLR residuals as a function of the Sun elongation angle (ε angle, the angle formed by Earth–spacecraft–Sun) for the four satellites. As expected, SLR residuals show an obvious linear systematic error with respect to the ε angle. Interestingly, CAST and SECM satellites show opposite patterns of SLR residuals with similar absolute value of the slope due to different stretched surfaces for the SECM (Z) and CAST (X) satellites. The systematic patterns of SLR residuals can be reduced when using the a priori box-wing model based on BDS-3 metadata or the empirical ECOM-2 (Yan et al. 2019; Li et al. 2020a; Springer et al. 2020).

3.3 Clock quality

3.3.1 Differences to GFZ solutions

Besides the orbits, the BDS-3 clock products with sampling of 30 s have also been released by GFZ since DOY 332, 2019. Hence, the WUM BDS-3 30 s clock offsets can be validated with those of GFZ by using the double-difference approach. Considering the good quality of the BDS-2 C11 clock (Zhao et al. 2017), it is selected as the reference clock, and the differences of other BDS-3 satellite clocks with respect to the C11 clock are formed to remove the AC-specific clock datum. Afterward, the clock of the same satellite pair from GFZ and WUM is further differenced and the STDevs of the double-difference clock corrections are calculated as indicators for clock quality, shown in Fig. 7. In general, the achieved mean STDev of clock differences is about 0.12 ns for the analyzed BDS-3 satellites. Similar as the orbits, the clock consistency is also related to the available tracking data of the satellites. The more data available, the better the achieved performance of the estimated clock corrections.

3.3.2 Linear clock fit

Furthermore, the quality of the satellite clocks can be represented by the RMS of the residuals after linear fit of the epoch-wise clock estimates for each day. As orbit errors are partly absorbed by the satellite clocks, the RMS of clock residuals represents not only the pure clock performance, but also some orbit errors (Sidorov et al. 2020). The linear clock fit (LCF) of all BDS-3 satellites is analyzed. However, for illustration, time series of LCF RMS for the selected representative satellites, i.e., C19 and C21 from CAST, C29 and C30 from SECM, are shown in Fig. 8. As reported by the TARC of CSNO, the RAFSs are used as the primary onboard clock for C19 and C21, whereas PHMs are primary for C29 and C30. It is clearly observed that LCF RMS of C19 shows a different pattern than C21. Similar as that of C29 and C30, the RMS of C19 LCF varies with the Sun-elevation angle, reaches the maximum when the Sun elevation above orbital plane is close to zero, and gradually decreases with

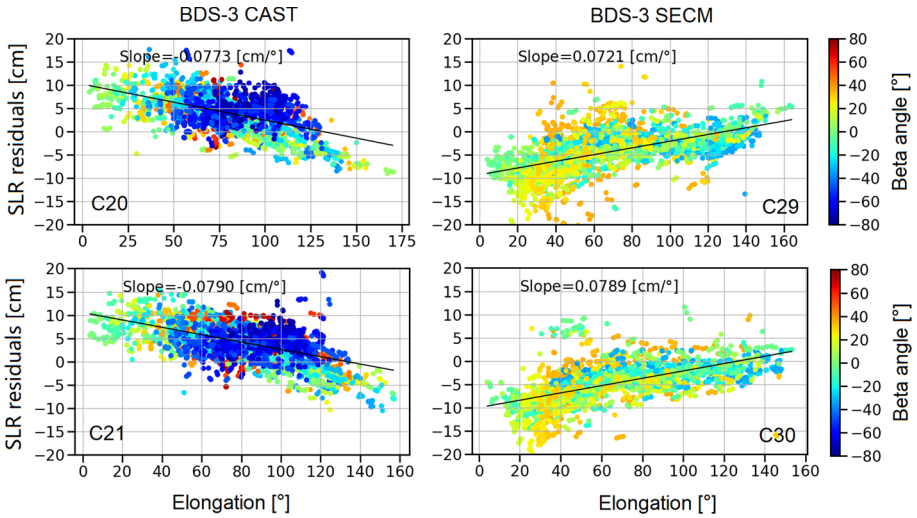

Fig. 6 SLR residuals of BDS-3 CAST (C20 and C21) and BDS-3 SECM (C29 and C30) satellites with respect to the Sun elongation angle

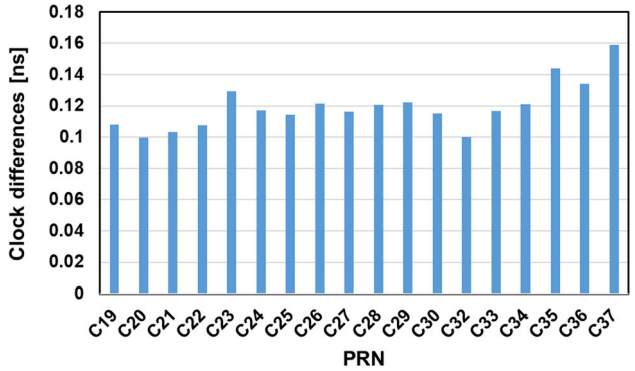

Fig. 7 STDev of the clock differences between GFZ and WUM clock products for different BDS-3 satellites

increasing Sun-elevation angle. This indicates orbit modeling deficiencies for BDS-3 as shown previously by SLR residuals. However, considering that C19 and C21 are in the same orbit plane, the LCF patterns could not be caused by non-conservative perturbations. Hence, it is very likely that the improved RAFS atomic clock is used as the primary frequency standard on C19. The LCF RMS value for the PHM clocks is approximately 4.8 cm, which is at the same level as the SLR residuals. However, the LCF RMS of RAFS clocks of C21 is larger than that of SLR residuals. Hence, the correlation between clock and SLR residuals for RAFS of C21 is not as obvious as that for PHMs and the improved RAFS of C19.

4 Improvements of BDS-3 solution

In this section, we consider several approaches to further improve BDS-3 orbit and clock solutions, i.e., the modeling of SRP, Earth albedo and antenna thrust based on the released metadata.

4.1 Antenna thrust

Antenna thrust is a radial acceleration caused by the transmission of navigation signals by GNSS satellites. For the computation of this acceleration, the total transmit power of the satellite has to be known. Steigenberger et al. (2018) provided the estimated transmit antenna power of the GPS, GLONASS, Galileo, BDS-2 and QZS-1 spacecraft. Besides, the Cabinet Office, Government of Japan also released the transmit power for all QZSS satellites. Those values have been already used for antenna thrust modeling by IGS and MGEX ACs for multi-GNSS data analysis. For BDS-3 satellites, CSNO does not disclose the transmit power, but Steigenberger and Thoelert (2020) measured the values, which are 310 W and 280 W for CAST and SECM MEO satellites, respectively. However, this information is not available for BDS-3 IGSO and GEO satellites. In this study, the transmit powers measured for MEO and CSNO released mass are used for antenna thrust modeling of BDS-3 MEO satellites.

With the strategy presented in Sect. 3.1, the orbit and clock solutions in 2019 were reprocessed based on the ECOM1 model with and without considering the antenna thrust. As the radial orbit offsets caused by the antenna thrust can be absorbed by the clock offsets, antenna thrust has minor effect on the LCF. Hence, only SLR validation is used to assess the impact of antenna thrust on satellite orbits. Table 4 lists the corresponding statistics of the SLR residuals. In comparison with the SLR validation for the official WUM orbit solutions, the reprocessed BDS-3 orbits with ECOM1 SRP model show slightly degraded performance for both CAST and SECM satellites. Comparison of the differences between

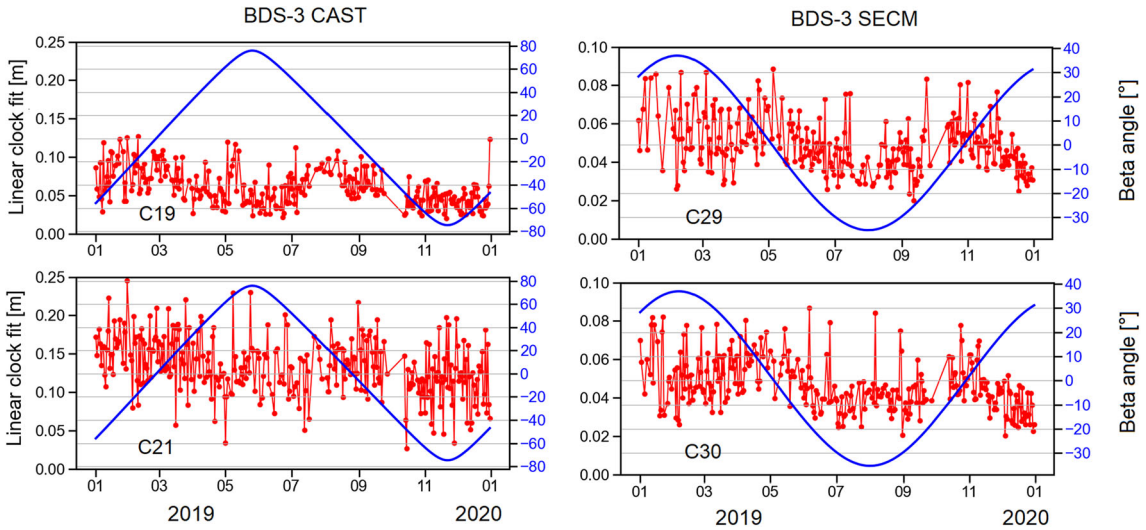

Fig. 8 The time series of linear clock fit residuals for the selected BDS-3 CAST C19 and C21 satellites, and BDS-3 SECM C29 and C30 satellites. (Note a different y-axis scale is plotted for the CAST and SECM satellites)

Table 4 Statistics of the SLR residuals for BDS-3 orbits with considering different non-conservative perturbations. (unit: cm; shift indicates the change of the mean offset due to antenna thrust and Earth albedo)

Solutions	PRN	Mean (cm)	STDev (cm)	RMS (cm)	Shift (cm)
ECOM1	C20	4.20	3.57	5.51	–
	C21	4.06	3.99	5.70	–
	C29	− 4.62	4.42	6.39	–
	C30	− 5.20	4.12	6.63	–
ECOM1 + Antenna thrust	C20	6.13	3.56	7.09	+ 1.93
	C21	5.99	3.97	7.18	+ 1.93
	C29	− 3.01	4.41	5.34	+ 1.61
	C30	− 3.60	4.08	5.44	+ 1.60
ECOM1 + Antenna thrust + Earth Albedo	C20	7.69	3.55	8.47	+ 1.56
	C21	7.53	3.87	8.47	+ 1.54
	C29	− 1.71	4.35	4.68	+ 1.30
	C30	− 2.33	4.02	4.65	+ 1.27
ECOM1 + Antenna thrust + Earth Albedo + a priori empirical SRP	C20	4.09	2.72	4.91	–
	C21	4.04	2.80	4.92	–
	C29	0.73	3.12	3.20	–
	C30	0.04	2.83	2.83	–

the two reprocessed solutions with and without antenna thrust clear shows that the antenna thrust has a minor impact on the STDevs of SLR residuals, but the mean of SLR residuals increases by about 1.93 cm and 1.60 cm for BDS-3 CAST and SECM MEO satellites, respectively. The orbit radius of the satellite decreases, which follows the conclusions of Steigenberger et al. (2018), as CAST satellites have higher transmit power with lower mass compared to SECM satellites. However, the shifts introduced by antenna thrust increase the biases in SLR residuals to around 6.0 cm for CAST MEO satellites, while the biases are about − 3.0 cm for SECM MEO satellites.

4.2 Earth albedo

Earth radiation pressure (ERP) or albedo is a non-gravitational perturbation caused by solar radiation reflected or reemitted by the Earth, and it generates an acceleration mainly along the radial direction. To model it with an analytical model, the geometrical and optical properties of the

spacecraft are necessary. For GPS and GLONASS, the ERP model developed by Rodriguez-Solano (2012b) has already been incorporated in IGS and IGS MGEX ACs routine analysis. The disclosure of dimensions and optical properties of Galileo and QZSS makes modeling of albedo for these satellites possible, and it has been already considered by most of IGS MGEX ACs. However, as aforementioned, CSNO does not disclose the specular and the diffuse reflection coefficients, nor the infrared radiation parameters, for BDS-3 satellites. Considering that the BDS-3 CAST satellites inherit the satellite bus from BDS-2, the optical coefficients of the same materials on BDS-3 satellites can be referred to those of BDS-2 listed in Chen et al. (2020). As reported by Li et al. (2020a), the triple-junction gallium arsenide solar cells are used for solar panels, and it has an absorption coefficient of about 0.92 without diffuse scattering. For the satellite body, CAST satellites employ a kind of multilayer with an absorption coefficient of 0.36 and a specular reflection coefficient of 0.0. In addition, the − X, + Y and − Y surfaces of CAST satellites are covered by optical solar reflectors (OSRs). The OSR has an absorption coefficient of 0.135 and a specular reflection coefficient of 0.865. The + X and − Z surfaces of CAST satellites are only covered by multilayers. As for the + Z surface of CAST satellites, it is reported to have an absorption coefficient of 0.92. For SECM satellites, all the six surfaces have the same absorption coefficient of 0.20. We assume that the OSRs are used; hence, a specular reflection coefficient of 0.80 is assumed as in Li et al. (2020a). With these parameters, a new solution based on ECOM1 SRP model with considering that antenna thrust and Earth albedo was determined.

Similar to antenna thrust, the Earth albedo also mainly affects the radial orbit component. Hence, only SLR is used for validation. The statistical results and the shifts with respect to the solution with antenna thrust modeling only are also listed in Table 4. It can be observed that inclusion of Earth albedo makes the satellites decrease in the radial direction by about 1.55 cm and 1.38 cm for BDS-3 CAST and SECM MEO satellites, and it has minor impacts on the STDevs of SLR residuals. However, it makes the biases in SLR residuals become much larger than 7.0 cm for CAST satellites, and it is about − 2.0 cm for SECM MEO satellites.

4.3 SRP model

Previous analysis with SLR residuals and LCF has already demonstrated that there are pronounced Sun-elongation-angle-dependent errors in orbits of BDS-3 MEO satellites due to the deficiency of the ECOM1 SRP model. Similar as Galileo and QZSS, this pattern is supposed to be caused by the cuboid shape of the satellites with relatively high area-to-mass ratio, and it can be reasonably reduced by empirical or semi-analytical models (Arnold et al. 2015; Montenbruck et al. 2015a). For BDS-3, Yan et al. (2019) calibrate the parameters of the semi-analytical model proposed by Montenbruck et al. (2015a), and Li et al. (2020a) assess the possibility to augment the empirical ECOM1 SRP model with a box-wing model. Both researches omit the antenna thrust and Earth albedo; hence, the determined orbit solutions have noticeable biases up to a few centimeters. As the reconstructed accelerations from the adjustable box-wing (ABW) model, partly absorbing antenna thrust and Earth albedo, are used to derive the model parameters in Yan et al. (2019), relatively smaller biases are shown in SLR residuals.

By considering the different performance of these SRP models, the better SRP models for BDS-3 CAST and SECM MEO satellites can be established by combining the ECOM1 and ABW models. To achieve this, the reconstructed SRP accelerations obtained from the ABW solution were used to develop an a priori SRP model by using a purely empirical parameter-fitting approach, as we did for BDS-2 GEO satellites (Wang et al. 2019a). Firstly, the ABW model developed by Rodriguez et al. (2012a) was used to fit the measurements with adjustable optical properties of illuminated surfaces as well as a scale parameter for solar panels, an empirical constant Y acceleration and solar panel lag angle. As correlations between the parameters of ABW are strong, reasonable results can be obtained only when a priori constraints are applied to most of these parameters. A priori constraints of 0.1 were applied to the optical coefficients with respect to the a priori values (CSNO 2019) in this study. Afterward, the SRP accelerations were reconstructed by orbit integration with 60-s interval using the orbital elements and SRP parameters determined from the ABW orbit solution. Secondly, the accelerations were decomposed in the DYB frame, which is aligned with the satellite-Sun direction and the nominal solar panel axis in yaw-steering mode. The decomposed accelerations were used as input to a spectral analysis. Figure 9 shows the amplitude spectra of the re-constructed SRP accelerations in the DYB frame for CAST C20 and SECM C30 satellites, respectively. The small and almost constant values in Y direction are not shown, as it can be absorbed by the Y0 parameter of ECOM1. It can be seen that the noticeable signals are quite similar for both C20 and C30 satellites. Besides 1-cpr (cycle-per-revolution) signal, the signals with amplitude above 1×10^{-10} m/s^2 are the even order in the D direction, whereas only odd-order signals show larger amplitude in the B axis. Similar patterns are also identified for other CAST and SECM MEO satellites.

Finally, the empirical SRP model can be derived based on the spectral analysis by selection of the periodic signals with amplitude above 1×10^{-10} m/s^2. For BDS-3 MEO satellites, the periodic signals of 1-cpr, 2-cpr and 4-cpr in D direction as well as 1-cpr and 3-cpr signals in B direction are selected for the empirical SRP model. Although the best fitting performance can be obtained using all cosine and sine terms, to

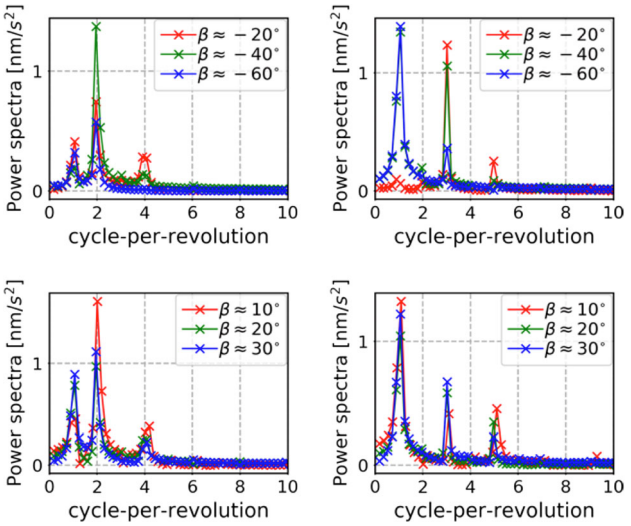

Fig. 9 Amplitude spectra of the reconstructed SRP accelerations decomposed into the D (left) and B (right) directions for BDS-3 CAST C20 (top) and SECM C30 (bottom) satellites

minimize the number of model parameters only cosine terms are selected in D and B directions as almost the same accuracy is achieved. Hence, the final formula can be expressed as:

$$\begin{aligned} a_{D,\mathrm{pri}} &= D_0 + D_{1c}\cos\mu + D_{2c}\cos 2\mu + D_{4c}\cos 4\mu \\ a_{B,\mathrm{pri}} &= B_{1c}\cos\mu + B_{3c}\cos 3\mu \end{aligned} \quad (1)$$

where μ is the orbital angle with respect to the midnight point, and D_0, D_{1c}, D_{2c}, D_{4c}, B_{1c} and B_{3c} are the parameters to be further estimated by fitting the reconstructed ABW acceleration in each axis. Clear β-angle-dependent variations in D_0, D_{2c} and B_{3c} could be observed, as shown in Fig. 10. Hence, they are further fitted with second-order polynomial function as their estimates show a clear quadratic correlation with β angle. Table 5 lists the estimated values for those parameters in Eq. (1) at 1 AU (Astronomical Unit).

With the proposed empirical SRP model as a priori to augment the ECOM1 model along with antenna thrust and Earth albedo, the orbit and clock solutions of BDS-3 satellites were redetermined. Unfortunately, the ambiguity fixing rate cannot be used as an effective indicators of SRP contribution, as it has been improved marginally. Besides, no noticeable impacts are observed for OBD. The similar phenomenon has been reported by Montenbruck et al. (2015a) for Galileo, as errors introduced in the stand-alone ECOM1 solution are highly correlated from one day to the next. Hence, besides SLR validation, the LCF as well as the estimates of the ECOM1 parameters are used to investigate the impact of the proposed a priori SRP model on orbit and clock solutions.

Figure 11 shows the SLR residuals with respect to the Sun elongation angle for the four BDS-3 satellites tracked by

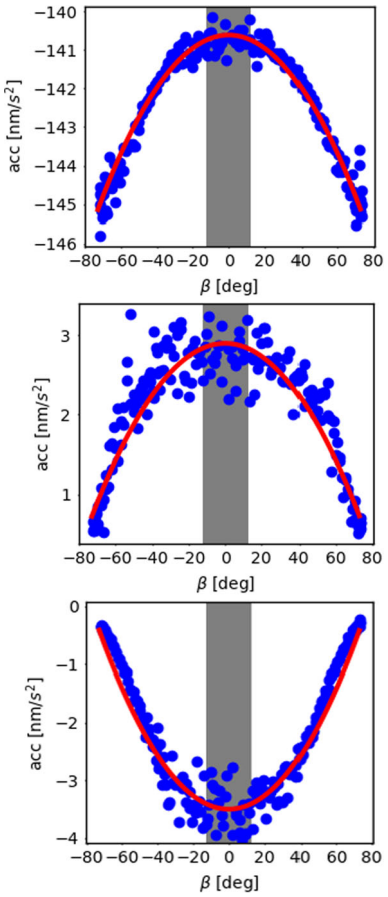

Fig. 10 Variations of the estimated parameters of the proposed model of SRP as a function of the β angle (D_0, top; D_{2c}, middle; B_{3c}, bottom)

ILRS. It is clearly observed that the Sun-elongation-angle-dependent errors have been almost completely removed, and the slope of the SLR residuals approaches zero. The statistical results are also listed in Table 4. In general, the biases in SLR residuals have been significantly reduced from about 7.6 cm to around 4.1 cm for CAST MEO satellites, while they are around 0.4 cm for SECM satellites. And the STDev reaches around 2.8 cm and around 2.9 cm for BDS-3 CAST and SECM MEO satellites, respectively. The proposed SRP model has already been incorporated in our routine WUM products with considering antenna thrust and Earth radiation pressure since June 12, 2020, and the validation with independent SLR data can be found at the IGS MGEX analysis webpage (see https://www.igs.org/mgex/analysis/#bd3-slr-residuals0450-ae6e).

Figure 12 shows the time series of LCF RMS of the BDS-3 MEO C19 and C30 satellites with and without employing the a priori SRP models. For satellites with PHMs as C30 the LCF RMSs are reduced by about 1 cm when using the a priori SRP model, particularly in the low Sun elevation angle region. Besides, a slight improvement is also identified for C19 with improved RAFS, whereas almost no changes are

Table 5 The estimated values for the parameters of the proposed a priori model for the BDS-3 CAST and SECM MEO satellites. (units: nm/s^2; β in degrees)

CAST MEOs	Value	SECM MEOs	Value
D_0	$-8.5\times10^{-4}\cdot\beta^2-140.0$	D_0	$1.8\times10^{-3}\cdot\beta^2-75.2$
D_{1c}	1.0	D_{1c}	0.8
D_{2c}	$-3.9\times10^{-4}\cdot\beta^2+2.9$	D_{2c}	$3.2\times10^{-3}\cdot\beta^2-5.2$
D_{4c}	−0.5	D_{4c}	−0.9
B_{1c}	2.3	B_{1c}	−3.5
B_{3c}	$5.8\times10^{-4}\cdot\beta^2-3.5$	B_{3c}	−1.4

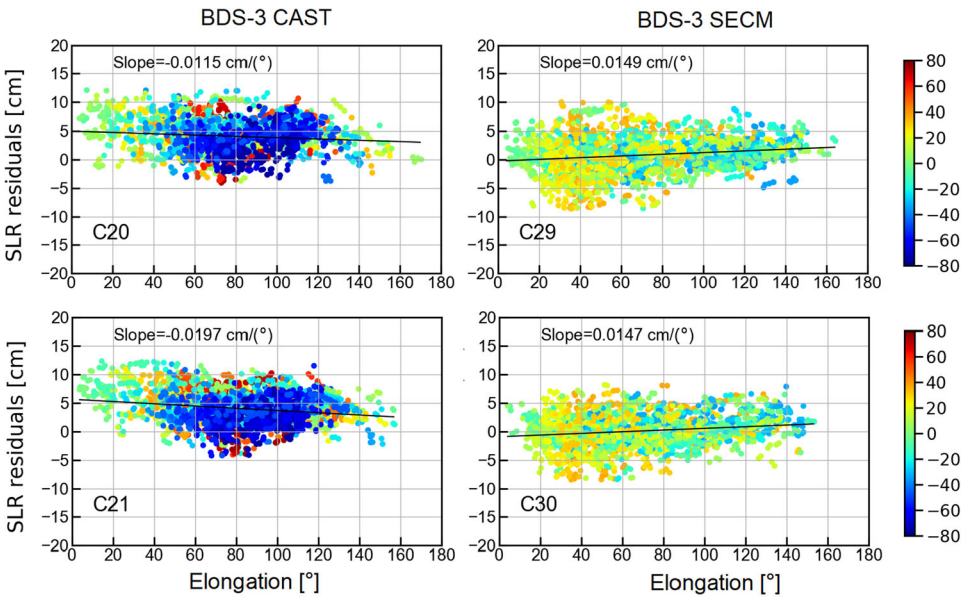

Fig. 11 SLR residuals for the redetermined orbits of BDS-3 CAST C20 and C21 as well as SECM C29 and C30 satellites with the proposed a priori SRP model to augment the ECOM1 model and antenna thrust as well as Earth albedo

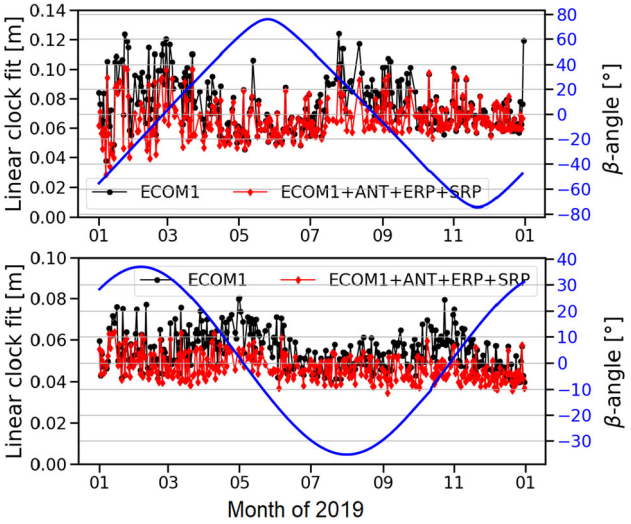

Fig. 12 LCF RMS time series of BDS-3 C19 (top) and C30 (bottom) satellite using ECOM1 with (red) and without (black) a priori SRP model

identified for the satellites with RAFSs. This is contributed to the fact that the noise of RAFS clock surpasses the orbit errors generated by mismodeling SRP perturbations. Although the LCF RMS is reduced with improved SRP model, there are still bumps in eclipse seasons, possibly caused by unmodeled thermal radiation like Galileo (Sidorov et al. 2019). In addition, compared with the LCF RMS of Galileo E19 carrying PHMs, the LCF of BDS-3 PHMs is larger by about 2 cm.

Figure 13 illustrates the daily estimates of four empirical parameters of the ECOM1 model, i.e., the constant along the D and B axis (D_0^* and B_0^*) as well as the 1-cpr parameters (B_{1c}^* and B_{1s}^*) along the B axis, with or without modeling the a priori SRP model for C20 and C30. It can be clearly observed for both satellites that the use of the a priori model essentially removes the β angle dependence or biases of the estimated D_0^* and B_0^*. The estimates of these two parameters as well as B_{1s}^* are near-zero and constant. However, B_{1c}^* shows a larger variation than the other two. Compared to the D_0^* estimates with the a priori model in Yan et al. (2019), our estimations are quite stable, in particular for high β angle. However, a residual variation of B_{1c}^* can still be recognized, particularly for C20. The B_{1s}^* estimates of other BDS-3 CAST MEO satellites in the same orbit plane as C20, i.e., C19, C21, C22, also show the same pattern. However, for other CAST MEO satellites in different orbit planes, slightly different patterns are obtained. This is also identified for

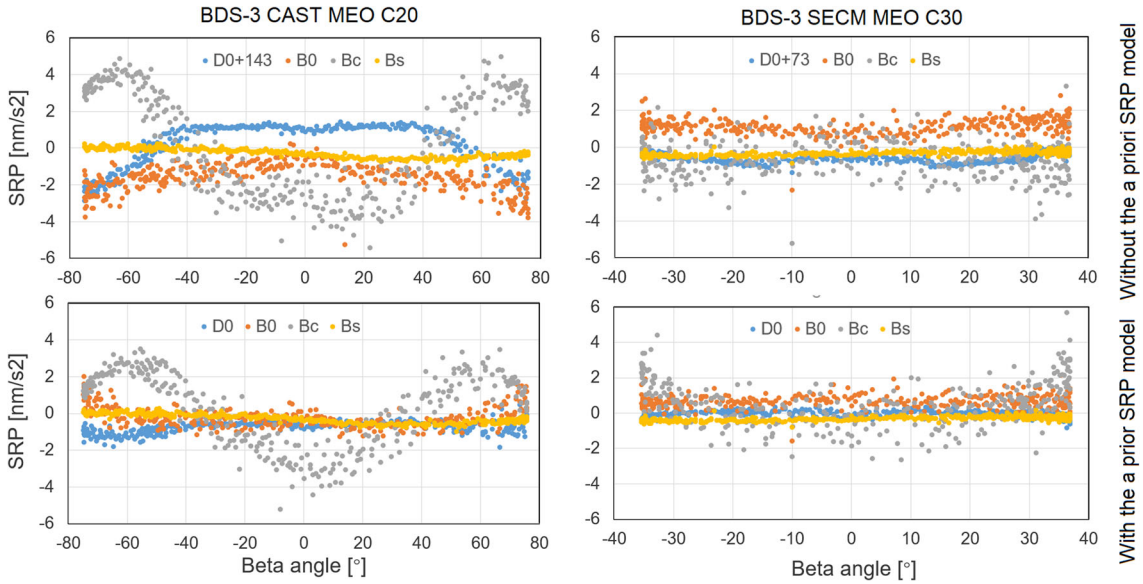

Fig. 13 Estimated ECOM1 model parameters of BDS-3 MEO satellites, i.e., C20 from CAST (left), C30 from SECM (right), without (up) and with (bottom) the proposed a priori empirical SRP model. Different parameters are marked with different colors

Galileo by Montenbruck et al. (2015a) with assuming that it may be caused by a slightly non-nominal orientation of the spacecraft or solar panel misalignment, but the root cause still needs further investigation.

5 Comparison with other SRP models

As mentioned previously, a priori box-wing models based on the published metadata (CSNO 2019) and on the calibrated optical coefficients (Duan et al. 2021) have been proposed for BDS-3 MEO satellites. Besides, the ECOM2 can also be applied (Yan et al. 2019). Duan et al. (2021) have already confirmed that the solution determined using ECOM1 in the case of the a priori box-wing model and an empirical constant acceleration in the along-track direction demonstrates the best performance. Hence, in this section, the performance of the proposed SRP model (denoted as ECOM1-FFT) is compared with that of the simple box-wing models based on the metadata released by CSNO (denoted as ECOM1-CSNO) and the adjusted coefficients reported by Duan et al. (2021) (denoted as ECOM1-ADJ). The same strategy as that used for the abovementioned reprocessing is used, except for the SRP model. Besides, an empirical constant acceleration in the along-track direction is also introduced. As antenna thrust and Earth radiation are considered by Duan et al. (2021) for the calibration of the coefficients, these are also included for the following solutions. Similarly, the SLR residuals, OBDs and 24-h predicted orbits are used for validations. For orbit prediction, because the Earth orientation parameters (EOPs) from the International Earth Rotation and Reference Systems Service are fixed, the predicted orbits are free of EOP errors.

Table 6 lists the results of SLR validation. In general, these SRP models can improve the orbit quality in comparison with ECOM1 by modeling antenna thrust and Earth radiation. The biases as well as the STDevs for C29 and C30 are reduced by about 1.0 m for ECOM1-CSNO. However, almost the same performance is achieved for C20 and C21. By using the adjusted values from Duan et al. (2021), noticeable improvements are obtained for C20 and C21, the STDevs are further reduced by about 0.8 and 0.6 cm, respectively, while the mean values are reduced by around 2.4 cm with respect to the ECOM1-CSNO solution. The STDevs of C29 and C30 decrease by about 0.2 cm, and an offset of around 2.0 cm can be identified for the average values of the SLR residuals. When the proposed model is used, the SLR residuals exhibit the smallest bias for the four satellites. However, the STDevs become slightly larger (by less than 0.2 cm) in comparison with those for ECOM-1-ADJ.

Table 7 lists the RMS of 3D orbit misclosures using each SRP model for different types of BDS satellites inside and outside the eclipse seasons. As the constant acceleration in the along-track direction is introduced, no noticeable degeneration is observed for the either type of satellite in the eclipse seasons. In comparison with those of the CAST satellites, the orbit misclosures of SECM satellites are larger by about 6.0 cm, mainly in the along-track direction. This might be caused by a larger deviation of the SECM PCOs from the CSNO published values (Zajdel et al. 2022). The assessment shows that the performance of the SRP models was similar, with a maximum difference of only about 1.8 cm. However,

Table 6 Statistics of SLR residuals for BDS-3 orbits using different SRP models. (unit: cm)

Solutions	PRN	Mean	STDev	RMS
ECOM1-CSNO	C20	7.61	3.40	8.33
	C21	8.05	3.26	8.68
	C29	− 0.27	3.04	3.05
	C30	− 1.00	2.71	2.90
ECOM1-ADJ	C20	5.33	2.58	5.92
	C21	5.64	2.66	6.24
	C29	1.66	3.01	3.44
	C30	0.94	2.78	2.94
ECOM1-FFT	C20	4.09	2.72	4.91
	C21	4.04	2.80	4.92
	C29	0.73	3.12	3.20
	C30	0.04	2.83	2.83

Table 7 RMS of 3D orbit boundary discontinuities using different SRP models (unit: cm)

SRP model	BDS-3 CAST		BDS-3 SECM	
	Non-eclipse	Eclipse	Non-eclipse	Eclipse
ECOM1-CSNO	12.0	12.5	18.4	20.3
ECOM1-ADJ	13.4	13.5	18.0	20.2
ECOM1-FFT	13.8	13.2	19.4	20.4

it is interesting to see that the ECOM1-FFT solution has a slightly lower quality except for the BDS-3 SECM satellites in the eclipse season.

To further assess the SRP models, BDS satellite orbits are predicted over 24 h on the basis of 1-day-arc solutions. The time period covers the whole year 2019. The orbits predicted using different SRP models are compared with the determined solution using the same SRP model. Table 8 shows RMSs of 3D orbit differences for each SRP model and satellite group. The CAST satellites still show better performance than the SECM satellites, particularly in the non-eclipse seasons. In case of the SRP models, similar as for the OBD results, the solutions obtained using different SRP models demonstrate similar performance. The ECOM1-FFT solution is the best for the BDS-3 SECM satellites both inside and outside the eclipse seasons.

6 Discussions and conclusions

In this study, we summarize the processing strategy and present the results of validation of the WUM BDS-3 orbit and clock solutions. The orbit accuracy in preliminary estimates is about 5–6 and 6–7 cm for CAST and SECM MEOs, respectively. The consistency between WUM and GFZ BDS-3 solutions is within 12 cm in 3D for orbits and 0.16 ns for clocks. However, the orbit and clock quality of BDS-3 satellites is noticeably affected by the number of tracking data available. Moreover, Sun-elongation angle-dependent errors are identified in the SLR residuals of those satellites. The RMSs of LCF of PHMs also demonstrate clear Sun-elevation-angle-dependent errors.

To reduce the systematic errors in orbits mentioned above, the improvements in the dynamic models of orbits, i.e., the SRP model, Earth albedo and antenna thrust, are addressed and highlighted as well. In general, on the basis of the measured transmit power as well as the metadata released by CSNO, the antenna thrust and Earth albedo are considered. This causes BDS-3 MEO satellites to shift along the radial direction by about -3.5 cm and -2.9 cm for CAST and SECM satellites, respectively. Furthermore, the a priori SRP models for BDS-3 CAST and SECM MEO satellites have been established on the basis of the ABW approach. By using this as an a priori model to augment the ECOM1, Sun-elongation-angle-dependent errors are significantly reduced for both CAST and SECM satellites. The STDevs of SLR residuals are around 3.0 cm. However, there are noticeable biases of up to about 4.0 cm for CAST MEO satellites. The biases are possibly caused by the LRA offsets released by the CSNO, as we have noticed that there is a bias of about 3.0 cm along the Z axis between data released by CSNO and those that we obtained from satellite manufacturers. With this correction, the biases can be reduced to less than 1.0 cm for satellites C20 and C21. On the other hand, considering the proposed a priori model,

Table 8 RMS of 3D orbit differences between 24-h predicted and determined solutions using different SRP models (unit: cm)

SRP model	BDS-3 CAST		BDS-3 SECM	
	Non-eclipse	Eclipse	Non-eclipse	Eclipse
ECOM1-CSNO	22.4	25.9	30.7	38.6
ECOM1-ADJ	23.1	27.7	31.7	36.1
ECOM1-FFT	23.2	26.6	29.3	34.2

the RMS of PHM LCF can be reduced by about 1.0 cm. In addition, the β angle dependence or bias of the estimated constant parameter along the D axis in the ECOM is removed. However, we would like to emphasize that the coefficients listed in Table 5 were derived by modeling antenna thrust and Earth albedo as well as assuming that the diffusion coefficients for each surface are zero. Particularly in the case of Earth albedo, unrealistic optical parameters were used. However, this has a limited effect on orbit solutions, as the a priori SRP model constructed using the ABW approach absorbs errors arising from mismodeling Earth albedo and antenna thrust. We compared the proposed SRP model with the simple box-wing model from other research groups. The OBDs and predicted orbits demonstrate almost the same performance. However, the solutions determined using the adjusted coefficients or the proposed model as an a prior to augment the ECOM-1 are slightly more accurate than those determined using the metadata released by CSNO.

With the abovementioned considerations the orbit accuracy reaches around 3.0 cm in the radial direction. This indicates the good performance of the BDS-3 constellation and suggests promising applications of BDS-3 satellites in geosciences.

Acknowledgements This study is sponsored by the National Natural Science Foundation of China (41974035), Young Elite Scientists Sponsorship Program by CAST (2018QNRC001), China Postdoctoral Science Foundation (2022M710478) and National Key R&D Program of China (2018YFC1503601). The IGS and iGMAS are greatly acknowledged for providing the Multi-GNSS products. We also thank the ILRS for providing laser ranging observations. We are grateful to the constructive comments and suggestions to improve the manuscript from Prof. Urs Hugentobler and three anonymous reviewers.

Author contributions JG worked on WUM processing, conceptualization, software, writing—original draft. CW performed SRP modeling—writing, review and editing. XX contributed to data reprocessing—review and editing. GC was involved in writing—review and editing. QZ helped in software and revision.

Data availability The BDS-3 tracking data are publicly available from IGS data centers, e.g., at the ftp site: ftp://cddis.gsfc.nasa.gov, where the SLR tracking data are also available. The WUM orbit and clock can be publicly assessed from IGS data centers. The reprocessed BDS-3 solutions are available upon request.

References

Arnold D, Meindl M, Beutler G, Dach R, Schaer S, Lutz S, Prange L, Sośnica K, Mervart L, Jäggi A (2015) CODE's new solar radiation pressure model for GNSS orbit determination. J Geod 89:775–791. https://doi.org/10.1007/s00190-015-0814-4

Beutler G, Brockmann E, Gurtner W, Hugentobler U, Mervart L, Rothacher M, Verdun A (1994) Extended orbit modeling techniques at the CODE processing center of the international GPS service for geodynamics (IGS): theory and initial results. Manuscr Geod 19(6):367–386

Chen Q, Yang H et al (2020) Solar radiation pressure modeling and application of BDS satellites. J Geod Geoinform Sci 3(2):45–52. https://doi.org/10.11947/j.JGGS.2020.0205

CSNO (2018) Development of the BeiDou navigation Satellite System, China Satellite Navigation Office. December, 2018. http://beidou.gov.cn/xt/gfxz/201812/P020190117356387956569.pdf

CSNO (2019) Satellite Information of BDS, China Satellite Navigation Office. http://en.beidou.gov.cn/SYSTEMS/Officialdocument/201912/P020200103556125703019.rar

Dilssner F (2017) A note on the yaw attitude modeling of BeiDou IGSO-6, November 2017. http://navigation-office.esa.int/attachments_24576369_1_BeiDou_IGSO6_Yaw_Modeling.pdf. Accessed 21 June 2020

Dilssner F, Springer T, Schönemann, Enderle W (2018) Initial orbit determination of third-generation BeiDou MEO spacecraft. In: IGS workshop 2018, 28 Oct–2 Nov 2018, Wuhan, China

Duan B, Hugentobler U, Selmke I, Marz S, Killian M, Rott M (2021) BeiDou satellite radiation force models for precise orbit determination and geodetic applications. IEEE Trans Aerosp Electron Syst. https://doi.org/10.1109/TAES.2021.3140018

Ge M, Gendt G, Dick G, Zhang FP (2005) Improving carrier-phase ambiguity resolution in global GPS network solutions. J Geod 79(1–3):103–110. https://doi.org/10.1007/s00190-005-0447-0

GSC (2017) Galileo Satellite Metadata, European GNSS Service Centre. https://www.gsc-europa.eu/support-to-developers/galileo-satellite-metadata

Griffiths J, Ray J (2009) On the precision and accuracy of IGS orbits. J Geod 83:277–287. https://doi.org/10.1007/s00190-008-0237-6

Guo J (2014) The impacts of attitude, solar radiation and function model on precise orbit determination for GNSS satellites. Ph.D. dissertation (in Chinese with English abstract), GNSS Research Center, Wuhan University, Wuhan, China

Guo J, Xu X, Zhao Q, Liu J (2016) Precise orbit determination for quad-constellation satellites at Wuhan University: strategy, result validation, and comparison. J Geod 90:143–159. https://doi.org/10.1007/s00190-015-0862-9

Guo J, Zhao Q, Xu X, Tao J, Zhang Q, Qu Z, Chen G, Wang C (2018) Real-time orbit and clock products at Wuhan University to support Multi-GNSS applications. IGS Workshop 2018, 29 October to 2 November, Wuhan, China

Jiao W, Liu Y (2014) International GNSS monitoring and assessment system (iGMAS) and latest progress, CSNC, 2014

Johnston G, Riddell A, Hausler G (2017) The international GNSS service. In: Teunissen PJ, Montenbruck O (eds) Springer handbook of global navigation satellite systems. Springer, Berlin, pp 967–982

Li X, Yuan Y, Zhu Y et al (2019) Precise orbit determination for BDS3 experimental satellites using iGMAS and MGEX tracking networks. J Geod 93:103–117. https://doi.org/10.1007/s00190-018-1144-0

Li X, Yuan Y, Zhu Y, Jiao W, Bian L, Li X, Zhang K (2020a) Improving BDS-3 precise orbit determination for medium earth orbit satellites. GPS Solut 24:53. https://doi.org/10.1007/s10291-020-0967-3

Li X, Zhu Y, Zheng K, Yuan Y, Liu G, Xiong Y (2020b) (2020b) Precise orbit and clock products of Galileo, BDS and QZSS from MGEX Since 2018: comparison and PPP validation. Remote Sens 12:1415

Lin X, Lin B, Liu Y, Xiong S, Bai T (2018) Satellite geometry and attitude mode of MEO satellites of BDS-3 developed by SECM. In: Proceedings of the ION GNSS 2018. Institute of Navigation, Miami, Florida, USA, September 24–28, pp 1268–1289. https://doi.org/10.33012/2018.16118

Liu J, Ge M (2003) PANDA software and its preliminary result of positioning and orbit determination. Wuhan Univ J Nat Sci 8(2B):603–609. https://doi.org/10.1007/BF02899825

Mi X, Sheng C, El-mowafy A, Zhang B (2021) Characteristics of receiver-related biases between BDS-3 and BDS-2 for five frequencies including inter-system biases, differential code biases, and differential phase biases. GPS Solut 25:113. https://doi.org/10.1007/s10291-021-01151-w

Montenbruck O, Steigenberger P, Hugentobler U (2015a) Enhanced solar radiation pressure modeling for Galileo satellites. J Geod 89(3):283–297. https://doi.org/10.1007/s00190-014-0774-0

Montenbruck O, Schmid R, Mercier F, Steigenberger P, Noll C, Fatkulin R, Kogure S, Ganeshan AS (2015b) GNSS satellite geometry and attitude models. Adv Space Res 56(6):1015–1029. https://doi.org/10.1016/j.asr.2015b.06.019

Montenbruck O, Steigenberger P, Prange L, Deng Z, Zhao Q, Perosanz F, Romero I, Noll C, Stürze A, Weber G, Schmid R, MacLeod K, Schaer S (2017) The multi-GNSS experiment (MGEX) of the international GNSS Service (IGS)—achievements, prospects and challenges. Adv Space Res 59:1671–1697. https://doi.org/10.1016/j.asr.2017.01.11

Pavlis N, Holmes S, Kenyon S, Factor J (2012) The development and evaluation of the earth gravitational model 2008 (EGM2008). J Geophys Res Solid Earth. https://doi.org/10.1029/2011jb008916

Pearlman MR, Noll CE, Pavlis EC, Lemoine FG, Combrink L, Degnan JJ, Kirchner G, Schreiber U (2019) The ilrs: approaching 20 years and planning for the future. J Geodesy 93(11):2161–2180. https://doi.org/10.1007/s00190-019-01241-1

Peng Y, Dai X, Lou Y, Gong X, Zheng F (2022) BDS-2 and BDS-3 combined precise orbit determination with hybrid ambiguity resolution. Measurement. https://doi.org/10.1016/j.measurement.2021.110593

Petit G, Luzum B (eds) (2010) IERS conventions. IERS Technical Note 36. Verlag des Bundesamts für Kartographie und Geodäsie, Frankfurt am Main. https://www.iers.org/IERS/EN/Publications/TechnicalNotes/tn36.html-1.htm?nn=94912 Accessed 22 Dec 2022

Rodriguez-Solano CJ, Hugentobler U, Steigenberger P (2012a) Adjustable box-wing model for solar radiation pressure impacting GPS satellites. Adv Space Res 49:1113–1128. https://doi.org/10.1016/j.asr.2012.01.016

Rodriguez-Solano C, Hugentobler U, Steigenberger P, Lutz S (2012b) Impact of earth radiation pressure on GPS position estimates. J Geod 86(5):309–317. https://doi.org/10.1007/s00190-011-0517-4

Springer T, Agrotis L, Dilssner F, Feltens J, van Kints M, Mayer V, Romero I, Enderle W, Schoenemann E, Zandbergen R (2020) The ESA/ESOC IGS analysis center technical report 2019. International GNSS service technical report 2019 (IGS annual report). IGS Central Bureau and University of Bern. https://doi.org/10.7892/boris.144003

Standish EM (1998) JPL planetary and lunar ephemerides, DE405/LE405, JPL IOM 312.F-98-048

Steigenberger P, Thoelert S (2020) Initial BDS-3 transmit power analysis (with BDS-2 gain pattern)

Steigenberger P, Thoelert S, Montenbruck O (2018) GNSS satellite transmit power and its impact on orbit determination. J Geod 92:609–624. https://doi.org/10.1007/s00190-017-1082-2

Sidorov D, Dach R, Prange L, JäggiA (2019) Enhanced orbit modelling of eclipsing Galileo satellites. In: 7th International colloquium on scientific and fundamental aspects of GNSS, 4–6 Sep. 2019, Zurich, Switzerland, Poster

Sidorov D, Dach R, Polle B, Prange L, Jäggi A (2020) Adopting the empirical CODE orbit model to Galileo satellites. Adv Space Res 66(12):15. https://doi.org/10.1016/j.asr.2020.05.028

Sośnica K, Zajdel R, Bury G, Bosy J, Moore M, Masoumi S (2020) Assessment of experimental IGS multi-GNSS combined orbits. GPS Solut 24:54. https://doi.org/10.1007/s10291-020-0965-5

Tang C, Hu X, Zhou S, Liu L, Pan J, Chen L, Guo R, Zhu L, Hu G, Li X, He F, Chang Z (2018) Initial results of centralizedautonomous orbit determination of the new-generation BDS satellites with inter-satellite link measurements. J Geod 92(10):1155–1169

Wang C, Guo J, Zhao Q, Liu J (2018) Yaw attitude modeling for BeiDou I06 and BeiDou-3 satellites. GPS Solut 22:117. https://doi.org/10.1007/s10291-018-0783-1

Wang C (2019) Solar radiation pressure modeling for BeiDou navigation satellites. Ph.D. dissertation (in Chinese with English abstract), GNSS Research Center, Wuhan University, Wuhan, China

Wang C, Guo J, Zhao Q, Liu J (2019a) Empirically derived model of solar radiation pressure for BeiDou GEO satellites. J Geod 93:791. https://doi.org/10.1007/s00190-018-1199-y

Wang C, Zhao Q, Guo J, Liu J, Chen G (2019b) The contribution of intersatellite links to BDS-3 orbit determination: model refinement and comparisons. Navigation

Xie X, Geng T, Zhao Q, Cai H, Zhang F, Wang X, Meng Y (2019) Precise orbit determination for BDS-3 satellites using satellite-ground and inter-satellite link observations. GPS Solut 23:40. https://doi.org/10.1007/s10291-019-0823-5

Yan X, Liu C, Huang G, Zhang Q, Wang L, Qin Z, Xie S (2019) A prior solar radiation pressure model for BeiDou-3 MEO satellites. Remote Sens 11:1605. https://doi.org/10.3390/rs11131605

Yang D, Yang J, Li G, Zhou Y, Tang C (2017) Globalization highlight: orbit determination using BeiDou inter-satellite ranging measurements. GPS Solut 21(3):1395–1404

Yang Y, Yang X, Li J, Yang C (2018) Progress and performance evaluation of BeiDou global navigation satellite system: data analysis based on BDS-3 demonstration system. Sci China Earth Sci 61(5):614–624

Yang Y, Gao W, Guo S, Mao Y, Yang Y (2019) Introduction to BeiDou-3 navigation satellite system. Navigation 2019:1–12. https://doi.org/10.1002/navi.291

Zajdel R, Steigenberger P, Montenbruck O (2022) On the potential contribution of BeiDou-3 to the realization of the terrestrial reference frame scale. GPS Solut 26:109. https://doi.org/10.1007/s10291-022-01298-0

Zhao Q, Wang C, Guo J, Wang B, Liu J (2017) Precise orbit and clock determination for BeiDou-3 experimental satellites with yaw attitude analysis. GPS Solut. https://doi.org/10.1007/s10291-017-0673-y

Zhao Q, Chen G, Guo J, Liu J, Liu X (2018) An a priori solar radiation pressure model for the QZSS Michibiki satellite. J Geod 92:109–121. https://doi.org/10.1007/s00190-017-1048-4

Zhang X, Wu M, Liu W, Li X, Yu S, Lu C, Wickert J (2017) Initial assessment of the COMPASS/BeiDou-3: new-generation navigation signals. J Geod 91(10):1225–1240. https://doi.org/10.1007/s00190-017-1020-3

Zhang B, Sun F, Jia X, Dai H, Xiao K (2019) Performance evaluation of BeiDou-3 onboard atomic clock. In: Book: China satellite navigation conference (CSNC) 2019 proceedings, vol 2, pp 368–375. https://doi.org/10.1007/978-981-13-7759-4_33

Zhou R, Hu Z, Zhao Q, Li P, Wang W, He C, Cai C, Pan Z (2018) Elevation-dependent pseudorange variation characteristics analysis for the new-generation BeiDou satellite navigation system. GPS Solut 22:60. https://doi.org/10.1007/s10291-018-0726-x